APPENDIX A: SUPPLEMENTAL INFORMATION FOR FLUID-ACOUSTIC SIMULATION

In Appendix A, supplementary descriptions of the fluid acoustic simulation using OpenFOAM are provided. In Sec. A, the spatial and temporal discretization schemes used in this paper are described. Section B describes the justification for the settings of the minimum mesh cell size and time step for the simulations in this paper.

A Spatial discretization and time discretization methods

In the fluid-acoustic simulation using OpenFOAM in this paper, second-order accurate spatial discretization schemes and the second-order implicit backward time scheme are used.[1] The discretization schemes for the divergence terms are shown in Table 1. ϕ is the mass flux, K is the kinetic energy, k_t is the turbulent kinetic energy, B is the sub-grid-scale stress tensor, and ν_{eff} is the effective kinematic viscosity. The discretization scheme for the gradient terms is set to 'Gauss linear,' and that for the Laplacian terms is set to 'Gauss linear corrected.'[1]

Divergent terms	Discretization schemes
$\boldsymbol{\nabla}\cdot(\phi v)$	Gauss LUST grad(U)
$\boldsymbol{\nabla}\cdot(\phi e)$	Gauss LUST grad(e)
$\boldsymbol{\nabla}\cdot(\phi K)$	Gauss linear
$\boldsymbol{\nabla}\cdot(\phi p)$	Gauss linear
$\boldsymbol{\nabla}\cdot(\phi k_t)$	Gauss limitedLinear 1
$\boldsymbol{\nabla}\cdot(\phi B)$	Gauss limitedLinear 1
$\boldsymbol{\nabla}\cdot B$	Gauss linear
$\boldsymbol{\nabla}\cdot(\rho\nu_{eff}\mathrm{dev}(T(\boldsymbol{\nabla}v)))$	Gauss linear

TABLE I. Discretization schemes for divergent terms

B Settings of minimum mesh cell size and time step

The minimum mesh cell size for the fluid-acoustic simulation in this paper is determined by referring to the results of the comparison between DNS and LES from prior 2D edge tone simulations.[2] The nozzle width and nozzle-edge distance for the edge-tone simulations are the same as in this paper (nozzle width = 1 mm, nozzle-edge distance = 5 mm). For LES, the calculations were carried out with a minimum mesh cell size of 0.05 mm and 0.1 mm, and it was confirmed that the DNS and LES results agree well in the low-Reynolds-number region where first mode oscillation occurs for both mesh cell sizes. Since the simulation of this paper is also in the low-Reynolds-number region, we set the minimum mesh cell size to 0.1 mm for our simulation. The time step $\Delta t = 5\times10^{-8}$ was determined based on the Courant number $(V_0 + c_0)\Delta t/\Delta x = 0.18$.

APPENDIX B: NUMERICAL VERIFICATION OF FDTD (2,4) SIMULATION

In Appendix B, we verify the accuracy of the simulation code for the FDTD(2,4) method. In Sec. B: A, a three-dimensional acoustic pulse propagation simulation is performed to verify the perfectly matched layer (PML) absorbing boundary condition. In Sec. B: B, acoustic scattering from a rigid cylinder is simulated to verify the solid boundary condition. In Sec. B: C, grid convergence is considered for the air-jet instrument simulation performed in the paper.

A Three-dimensional acoustic pulse propagation

In this section, a simulation is performed of a typical benchmark problem in computational acoustics, the three-dimensional Gaussian pulse propagation. The analytical solution, which can be obtained by solving the linearized Euler equations using the Fourier-Bessel transform,[3] is as follows:

$$p(r,t) = \frac{p_0}{\beta}\int_0^\infty \exp\left(-\frac{\xi^2}{4\alpha}\right)\cos\left(c_0\xi t\right) j_0(\xi r)\xi^2 d\xi, \quad (1)$$

where $\beta = 2\alpha\sqrt{\pi\alpha}$ and $j_0(z) = \sin(z)/z$ is the zeroth-order spherical Bessel function of the first kind. The parameters are set as follows: $p_0 = 0.001$; $c_0 = 1/\sqrt{3}$; $\alpha = \ln 2/10^2$.

The total grid size of the simulation is 200 × 200 × 200, and the origin is set at the center of the domain $(x, y, z = 0)$. As an initial condition, the initial pressure is set as $p = p_0\exp(-\alpha r^2)$, where r is the distance from the origin. The calculation time step is set as $\Delta t = 0.1$, and the equally spaced grid size is $\Delta x = 1$. The number of PML layers is 20, and the attenuation coefficient is set as $\eta(x) = \eta_{max}(x/20)^n$, where the parameters are set as follows: $\eta_{max} = 1.5$; $n = 4$.

Figure 1 compares the pressure along the horizontal x-axis $(0 \le x \le 80, y = 0, z = 0)$ obtained by the simulation with the analytical solution at typical time steps. As shown in the figure, the simulation result is in excellent agreement with the analytical solution.

To investigate the magnitude of the acoustic waves reflected back into the physical domain, the time evolution of the residual pressure L_p on the horizontal x-axis is calculated, using the definition,

$$L_p = \left(\frac{1}{N_x}\sum_i^{N_x} p_i^2\right)^{1/2}. \quad (2)$$

Figure 2 depicts time evolution of the residual pressure on the horizontal axis $(0 \le x \le 80, y = 0, z = 0)$. As shown in the inset of the figure, there is a detectable influence due to the reflection around the time range $150 < t < 350$, but L_p is two orders of magnitude smaller than the initial value and negligible. This confirms that the absorbing boundary condition is working effectively.

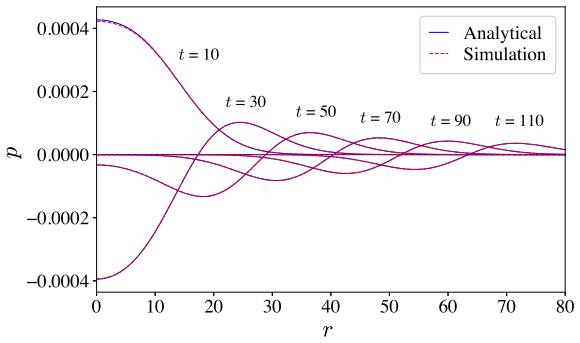

FIG. 1. Pressure distribution of three-dimensional Gaussian pulse propagation along the horizontal axis.

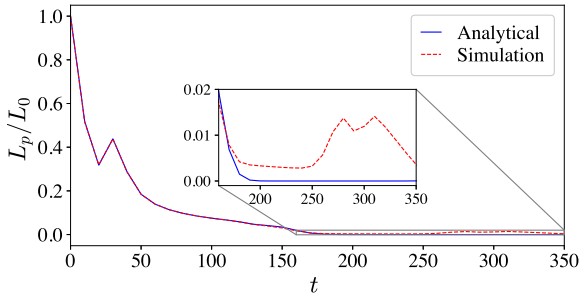

FIG. 2. Time evolution of residual pressure $L_p/L_p(0)$ on the horizontal axis.

B Acoustic scattering from a rigid cylinder

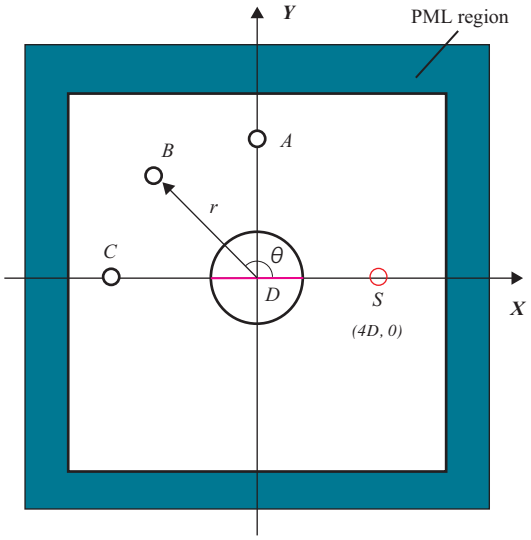

FIG. 3. Schematic of the cylinder scattering problem.

To verify the solid boundary condition, the benchmark problem of wave scattering by a circular cylinder is considered.[4] The schematic of the problem configuration is shown in Fig. 3.

In the simulation domain $-20.5 \le (x, y) \le 20.5$, the Gaussian pulse $p = \exp\{-\ln 2(r_s^2/0.2^2)\}$ is initially located around the point $S\,(4D, 0)$, where r_s is the distance from the point S, and $D = 1$ is the cylinder diameter. The sampling points at $r = 5$ are set as follows: point $A(\theta = 90°)$; point $B(\theta = 135°)$; point $C(\theta = 180°)$. The equally spaced grid size is $\Delta x = 0.02$, and the calculation time step is set as $\Delta t = 0.005$, and the sound speed is set as $c_0 = 1$. The PML region is set in the same way as in the previous section.

The analytical solution can be obtained by the superposition of the solution of velocity potential ϕ for the incident and reflected waves. After correcting some errors found in the original publication[4], it is given by the following equation:

$$p(r,\theta,t) = -\frac{\partial \phi}{\partial t} = -\frac{\partial}{\partial t}\left(\phi_i + \phi_r\right)$$
$$= \mathrm{Re}\left\{\int_0^\infty \left(A_i(r,\theta,\omega) + A_r(r,\theta,\omega)\right)\omega e^{-i\omega t} d\omega\right\}, \quad (3a)$$

$$A_i(r,\theta,w) = -\frac{e^{-b\omega^2/4b}}{2b} J_0\left(\omega\sqrt{r^2 + x_s^2 - 2rx_s\cos\theta}\right), \quad (3b)$$

$$A_r(r,\theta,w) = -\frac{e^{-b\omega^2/4b}}{2b}\sum_{k=0}^{\infty}\left[\frac{\varepsilon_k H_k(r\omega)\cos(k\theta)}{2k\pi\cdot H_k(\omega/2) - \pi\omega\cdot H_{k+1}(\omega/2)}\right] \cdot \int_0^\pi \omega\frac{(0.5 - x_s\cos(\eta))}{\sqrt{0.25 + x_s^2 - x_s\cos(\eta)}} \times J_1\left(\omega\sqrt{0.25 + x_s^2 - x_s\cos(\eta)}\right)\cos(k\eta)d\eta, \quad (3c)$$

where J_0, J_1 are the zeroth and first-order Bessel functions of the first kind and H_k is the kth-order Hankel function of the first kind ($\varepsilon_0 = 1$ and $\varepsilon_k = 2$ for $k \neq 0$).

Figure 4 depicts the time-series of pressure obtained by the simulation at the sampling points compared with the analytical solution. The results are in very good agreement, confirming the validity of the solid boundary condition.

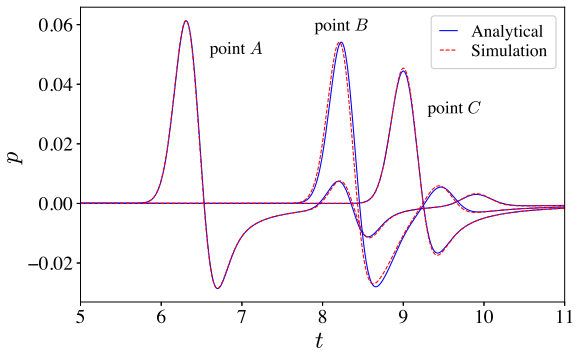

FIG. 4. Time-series of pressure at sampling points.

C Grid convergence of the air-jet instrument simulation

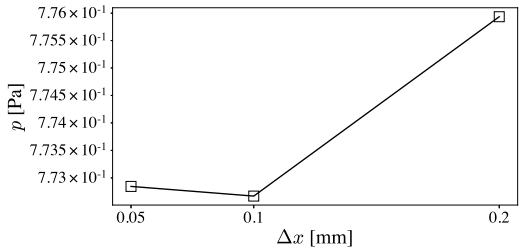

FIG. 5. Dependence of pressure value on grid cell size, in air-jet instrument simulation.

In this section, we discuss the grid convergence of the simulation of the air-jet instrument performed in the paper. The setup of the simulations in this section are the same as in the paper, but the grid size is varied while keeping the Courant number equivalent, and the inlet frequency is set as $f_1 = 850$ Hz.

The simulations were performed on the high performance computing cluster ITO (subsystem B)[5] with 4 nodes. For the multi-node parallelization, mSMS,[6] which is a page-based distributed shared memory system, is used.[7]

Figure 5 shows the values of pressure calculated for three grid sizes at the sampling point c defined in the paper and at time $t = 0.0006$ s, corresponding to the first positive peak of the sound wave emitted outside the instrument. As shown in the figure, the difference between the results for the grid size of 0.1 and 0.05 mm is very small, about 10^{-4}, confirming the validity of the grid size $\Delta x = 0.1$ mm adopted in the paper.

[1]The OpenFOAM Foundation, "Openfoam v5 user guide" , https://cfd.direct/openfoam/user-guide-v5/ , Last accessed on September 17, 2020.

[2]S. Iwagami, T. Kobayashi, K. Takahashi, and Y. Hattori, "Reproducibility of mode transition of edge tone with DNS and LES," in *Proceedings of the 23rd International Congress on Acoustics: Integrating 4th EAA Euroregio 2019*, International Commission for Acoustics (ICA) (2019), pp. 5573–5579.

[3]C. Bogey and C. Bailly, "Three-dimensional non-reflective boundary conditions for acoustic simulations: far field formulation and validation test cases," Acust. Acta Acust. **88**, 10 (2002).

[4]C. K. W. Tam and J. C. Hardin, eds., *Second Computational Aeroacoustics (CAA) Workshop on Benchmark Problems*, NASA CP-3352 (1997).

[5]Research Institute for Information Technology, Kyushu University, "Introduction of ITO" , https://www.cc.kyushu-u.ac.jp/scp/eng/system/ITO/01_intro.html , Last accessed on October 5, 2020.

[6]H. Midorikawa, K. Kitagawa, and Y. Sakaguchi, "mSMS: PGAS Runtime with Efficient Thread-based Communication for Global-view Programming," in *2019 IEEE International Conference on Cluster Computing* (2019).

[7]R. Tabata, H. Midorikawa, and K. Takahashi, "Performance evaluation of acoustic FDTD(2,4) method using distributed shared memory system mSMS," in *International Conference on High Performance Computing in Asia-Pacific Region* (2020).